Journal of Power Sources 224 (2013) 59–65

Contents lists available at SciVerse ScienceDirect

Journal of Power Sources

journal homepage: www.elsevier.com/locate/jpowsour

Microwave-assisted hydrothermal synthesis of vanadium oxides for Li-ion supercapacitors: The influences of Li-ion doping and crystallinity on the capacitive performances

Jing-Mei Li, Kuo-Hsin Chang, Tzu-Ho Wu, Chi-Chang Hu*

Department of Chemical Engineering, National Tsing Hua University, No. 101, Section 2, Kuang-Fu Road, Hsin-Chu 30013, Taiwan

HIGHLIGHTS

- ► $VO_x \cdot nH_2O$ with excellent capacitive behavior can be synthesized rapidly by an MAHS method.
- ► The crystal size and spacing distance of two adjacent layers are affected by the MAHS temperature and adding LiCl.
- ► The above two factors show great influences on the Li-ion intercalation capacity and rate.
- ► Doping Li ions into $VO_x \cdot nH_2O$ enlarges the spacing distance of adjacent layers and crystal size of $VO_x \cdot nH_2O$.
- ► Doping Li ions into $VO_x \cdot nH_2O$ enhances its specific capacitance and prolongs its cycle life.

ARTICLE INFO

Article history:
Received 19 March 2012
Received in revised form
30 August 2012
Accepted 3 September 2012
Available online 3 October 2012

Keywords:
Microwave
Hydrothermal synthesis
Lithium ion
Vanadium oxide
Supercapacitor

ABSTRACT

Vanadium oxides ($VO_x \cdot nH_2O$) with long cycle-life for Li-ion supercapacitors have been successfully synthesized by means of the microwave-assisted hydrothermal synthesis (MAHS) method, a faster and more energy-saving method than the conventional hydrothermal synthesis. Such oxides show capacitor-like, lithium-ion intercalation/de-intercalation responses in aqueous media. Although electrochemical activation is required to reveal the capacitor-like behavior of $VO_x \cdot nH_2O$, doping Li ions by adding LiCl into the precursor solution not only effectively shortens the activation time but also enhances the specific capacitance of $VO_x \cdot nH_2O$. This kind of materials shows the promising application potential in the aqueous-based Li-ion supercapacitors. X-ray diffraction (XRD), Raman spectroscopic, and X-ray photoelectron spectroscopic (XPS) analyses are employed to identify the fine tune-up in microstructures of various $VO_x \cdot nH_2O$.

1. Introduction

Vanadium oxides in multiple oxidation states/various forms with layered structures have been found to show redox intercalation ability for various cations [1–3]. Hence, many vanadium oxides are considered as important electrode materials in the electrochemical energy storage applications, such as lithium-ion batteries (LIBs) [4] and electrochemical capacitors (ECs) [5,6]. However, the intrinsic requirements for rechargeable batteries and ECs are different [7–10]. For example, ECs, also called supercapacitors or ultracapacitors, generally show the high power and long cycle-life characteristics with an acceptable energy density [7,9,11]. How to improve the electron conductivity and the ion diffusion/penetration rate and to inhibit the degradation of electrode materials are the major considerations in developing an ideal electrode material for such applications [12,13]. Moreover, the redox reactions of electrochemically active materials often involve the superficial region in order to ensure the excellent electrochemical reversibility for ECs [8], leading to a lower energy density in comparison with batteries. While rechargeable batteries usually show much higher energy densities by utilizing the bulk phase of electroactive materials (e.g., the Li-ion intercalation capability of vanadium oxides). Consequently, the low ion-diffusion rate within the bulk phase of active materials generally limits the power performance of devices [13,14] although power-oriented LIBs [13–16] have been developed for the usage in hybrid and pure electric vehicles (HEV and EV) recently. On the other hand, all the above concepts and viewpoints

* Corresponding author. Tel./fax: +886 3 5736027.
E-mail address: cchu@che.nthu.edu.tw (C.-C. Hu).
URL: http://mx.nthu.edu.tw/~cchu/

0378-7753/$ – see front matter © 2012 Elsevier B.V. All rights reserved.
http://dx.doi.org/10.1016/j.jpowsour.2012.09.007

agree that tuning/designing a desirable microstructure of electrochemically active materials for meeting the intrinsic requirements of individual electrochemical energy storage system is the key to enhance their respective performances.

In order to meet the requirements for the high-power ability, acceptable energy density, and very long cycle-life with an improved energy storage/delivery efficiency of ECs [7,9,11], developing an effective method for tuning the microstructure of vanadium oxides is very important. Such synthesis methods are not only important to the energy storage systems but also very interesting to other applications, e.g., catalysts, smart windows [17–19], and semiconductors [20]. Several wet chemical methods have been proposed to synthesize vanadium oxides, including sol–gel [17,21], hydrothermal [19,22–30], reverse micelle [31,32], and electrochemical deposition [5,6,33,34], etc. While it is still lack of full understanding on any method for effectively controlling/tuning the microstructures of crystalline vanadium oxides although hydrothermal synthesis with a long reaction time (sometimes even longer than 1 week) seems to be widely studied [19,22–29,35]. From the practical application viewpoint, the cycle-life issue is still a big challenge for vanadium oxides in ECs due to the structure collapse or phase transition during intercalation/de-intercalation of Li ions [14,36,37], although vanadium oxides with the well-known layered structure showed a promising applicability to LIBs [25,38–40] and ECs [5,6,23,35,41,42]. Hence, developing new/improving existed methods for manufacturing vanadium oxides with properties meeting the above requirements is very important.

In general, the microwave-assisted hydrothermal synthesis (MAHS) method is a homogeneous heating process and creates the possibilities in obtaining new and modified forms of materials [43,44] through the direct energy transfer from the water molecules to the precursors in comparing with conventional hydrothermal synthesis. Such a unique "molecular heating" method has been shown to provide several merits in materials preparation, e.g., rapid volumetric heating, high reaction rate, short reaction time, high reaction selectivity, and energy saving [43,44]. Recently, microwave-assisted hydrothermal/solvothermal methods have been tried to fabricate metal oxides [45–47] although they have been widely applied to organic synthesis. Consequently, it is still lack of detailed discussion on the fabrication of metal oxides through such interesting methods. In this work, vanadium oxides were proposed to be synthesized by means of the MAHS route for the EC application.

In our previous work [5,6,33,34], hydrous vanadium oxides deposited at potentials equal to/positive than 0.4 V showed promising capacitive performances in aqueous media containing concentrated Li ions. Such vanadium oxides have been found to possess highly reversible Li-ion intercalation/de-intercalation behavior in 12 M LiCl between −0.2 and 0.8 V. Since the tunnels of Li-ion diffusion should be affected by the crystallinity of vanadium oxides [14,48], this work employs the MAHS process to synthesize vanadium oxide nanocrystals in order to shorten the Li-ion diffusion length. Moreover, this work demonstrates the idea that doping of Li ions can tune the Li-ion diffusion tunnels within vanadium oxide nanocrystals in order to enhance the Li-ion intercalation/de-intercalation rate for the application of ECs.

2. Experimental

All vanadium oxides (denoted as $VO_x \cdot nH_2O$) were synthesized by means of the microwave-assisted hydrothermal synthesis (MAHS) method. An aqueous solution containing 25 mM $VOSO_4 \cdot nH_2O$ was utilized as the main precursor solution, and hydrogen peroxide was added to adjust the V^{4+}/V^{5+} ratio equal to one. LiCl was used as the lithium-ion source in the precursor solution for doping Li ions into the oxides. The pH value of the precursor solutions was adjusted to 2.7 with 1 M H_2SO_4 and 2 M NaOH. Synthesis of $VO_x \cdot nH_2O$ was performed through a microwave reactor, Discover SP™ (CEM, USA), with temperatures equal to 140, 180 or 200 °C for 10 min. The products were washed with deionized water several times.

The chemical environments of $VO_x \cdot nH_2O$ were analyzed through XPS by means of an ESCA210 spectrometer (Kratos Axis Ultra DLD). The XRD patterns were obtained from an X-ray powder diffractometer (CuKα, Ultima IV, Rigaku) at an angle speed of 4° (2θ) min^{-1}. Raman spectra were measured using a 3D nanometer scale Raman PL microspectrometer (Tokyo Instruments, INC) with 632.8 nm radiation of a HeNe laser, which was focused in a circle area less than 1 μm in diameter. The doping mount of Li ions into $VO_x \cdot nH_2O$ was determined by means of an inductively coupled plasma–mass spectrometer (ICP–MS, SCIEX ELAN 5000), Auger electron spectrometer (AES, ULVAC-PHI AES 650), and Time-of-Flight Secondary Ion Mass Spectrometer (ToF-SIMS, TOF.SIMS IV). The electrochemical properties of $VO_x \cdot nH_2O$ were examined by an electrochemical analyzer system, CHI 633c (CH Instruments, USA) in a three-compartment cell. An Ag/AgCl electrode was utilized as the reference and a piece of platinum gauze was employed as the counter electrode. A Luggin capillary was used to minimize errors due to *iR* drop in the electrolytes.

All solutions used in this work were prepared with deionized water produced by a reagent water system (Milli-Q SP, Japan) at 18 MΩ cm. All reagents, not specified, without further purification are Merck, GR. The electrolyte, 12 M LiCl, used for electrochemical characterization was maintained at 25 °C and degassed with purified N_2 for 25 min before measurements. This nitrogen flow was passed over the solutions during the measurements. The solution temperature was maintained at the specified temperature by a water thermostat (Haake DC3 and K20).

3. Results and discussion

3.1. Effects of the MAHS temperature on the electrochemical behavior of $VO_x \cdot nH_2O$

The electrochemical properties of various $VO_x \cdot nH_2O$ samples prepared at different MAHS temperatures were examined in 12 M LiCl between −0.2 and 0.8 V. Curves 1–3 in Fig. 1 show the typical electrochemical behavior measured at a scan rate of 25 mV s^{-1} for

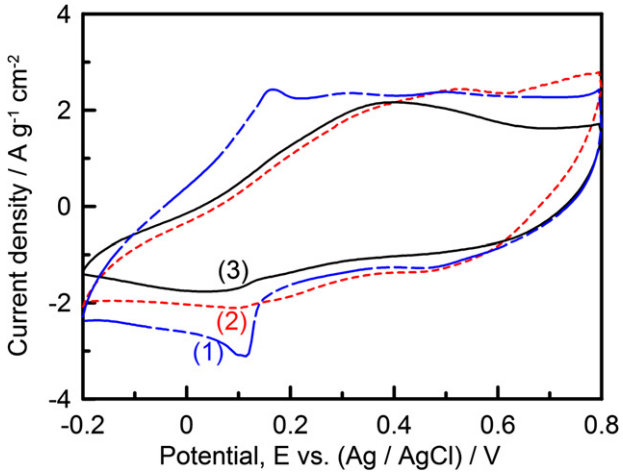

Fig. 1. Cyclic voltammograms (the 2nd cycle) of $VO_x \cdot nH_2O$ synthesized by means of the MAHS method at (1) 140, (2) 180, and (3) 200 °C.

as-prepared $VO_x \cdot nH_2O$ fabricated by the MAHS method at 140, 180, and 200 °C, respectively. On curve 1, there is a pair of small redox peaks with the anodic and cathodic peak potentials equal to 0.16 and 0.11 V respectively. Very broad waves are visible on both positive and negative sweeps at potentials positive than these peaks. Interestingly, no obvious redox peaks are visible on curves 2 and 3 corresponding to the $VO_x \cdot nH_2O$ synthesized at 180 and 200 °C, respectively. Note that the voltammetric charges gradually decrease with increasing the MAHS temperature. Moreover, curve 1 is more symmetric in shape than curves 2 and 3, indicating higher electrochemical reversibility. All the above results reveal that among the above three $VO_x \cdot nH_2O$ materials, the sample synthesized at 140 °C shows the highest capacity and the best electrochemical reversibility for Li-ion intercalation/de-intercalation.

After 500-cycle CV activation between −0.2 and 0.8 V at 25 mV s^{-1} in 12 M LiCl, the above three $VO_x \cdot nH_2O$ materials show much more improved capacitor-like responses (see Fig. 2). A pair of redox peaks around 0.1 V clearly observed on all CV curves is highly symmetric in shape, especially for curves 1 and 2. The peak potentials on all curves are approximately the same, suggesting an identical Li-ion intercalation/de-intercalation reaction. A comparison of Figs. 1 and 2 reveals that the electrochemical reversibility of Li-ion intercalation/de-intercalation within $VO_x \cdot nH_2O$ is improved by the electrochemical activation step, judged by the symmetric *i*–*E* responses and the sharp change from anodic to cathodic current when the sweep direction is changed at the upper potential limit of CV. Note that $VO_x \cdot nH_2O$ synthesized at 140 °C still shows the best capacitive performances among all $VO_x \cdot nH_2O$ materials, according to the current density and symmetry of CV. From the above results and discussion, the MAHS temperature shows a significant influence on the Li-ion intercalation/de-intercalation ability of $VO_x \cdot nH_2O$ in concentrated LiCl solutions. Clearly, the step of electrochemical activation is necessary for $VO_x \cdot nH_2O$ prepared by means of the MAHS method, probably due to the better crystallinity of these $VO_x \cdot nH_2O$ materials in comparison with that prepared by anodic deposition. Furthermore, the much lower $C_{S,T}$ (274 F g^{-1}) of $VO_x \cdot nH_2O$ prepared by means of the MAHS method in comparison with that (882 F g^{-1}) of $VO_x \cdot nH_2O$ prepared by anodic deposition can ascribe to its the better crystallinity (see below).

Fig. 3 shows the dependence of the specific capacitance ($C_{S,T}$) on the MAHS temperature and cycle number. On curves 1 and 2, $C_{S,T}$ of $VO_x \cdot nH_2O$ synthesized at 140 and 180 °C reaches their respective highest value (176 and 145 F g^{-1}) at the cycle numbers equal to 2500 and 3000, respectively. The $C_{S,T}$ of $VO_x \cdot nH_2O$ fabricated at 140 °C

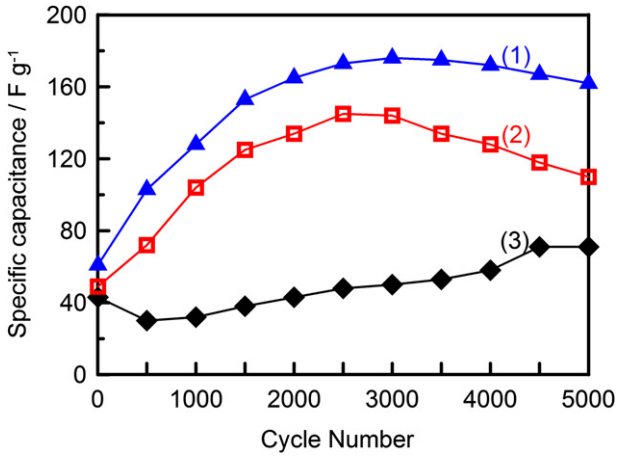

Fig. 3. Dependence of the specific capacitance on the cycle number for $VO_x \cdot nH_2O$ synthesized by means of the MAHS method at (1) 140, (2) 180, and (3) 200 °C.

decreases slightly to 92% of its highest value after the 5000-cycle test, revealing an excellent stability. Such excellent cycle life of $VO_x \cdot nH_2O$ for Li-ion intercalation/de-intercalation in aqueous media is never found before. On curve 2, however, $C_{S,T}$ declines obviously after passing the maximal value and 76% retention is obtained for this 5000-cycle test. The $VO_x \cdot nH_2O$ produced at 200 °C shows the highest $C_{S,T}$ value between 4500 and 5000 cycles. All the above results and discussion indicate that the MAHS temperature shows significant influences on the rate and capacity of Li-ion intercalation/de-intercalation as well as the cycle life of $VO_x \cdot nH_2O$ in the Li-ion supercapacitor application.

3.2. Effects of Li-ion doping on the electrochemical properties of $VO_x \cdot nH_2O$

Figs. 4 and 5 show the effects of Li-ion doping on the voltammetric behavior of $VO_x \cdot nH_2O$ synthesized at 140 °C. In Fig. 4, the *i*–*E* responses of $VO_x \cdot nH_2O$ without and with Li-ion doping (without electrochemical activation) are very similar in shape, while the voltammetric current density in the whole potential region of investigation is obviously enhanced by the Li-ion doping. The former result suggests that the crystalline phase of $VO_x \cdot nH_2O$ is not changed by the Li-ion doping. The latter phenomenon indicates

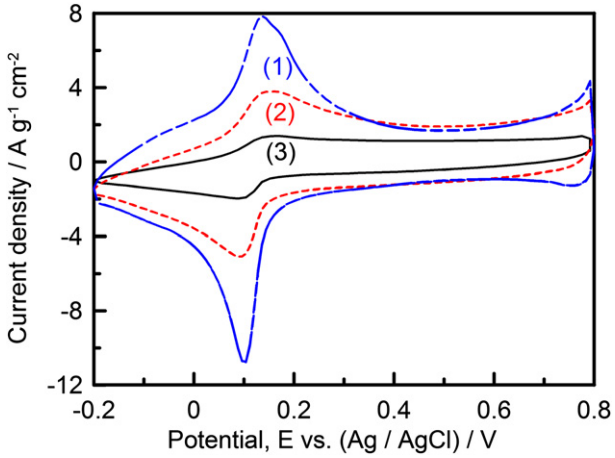

Fig. 2. Cyclic voltammograms (the 500th cycle) of activated $VO_x \cdot nH_2O$ synthesized by means of the MAHS method at (1) 140, (2) 180, and (3) 200 °C.

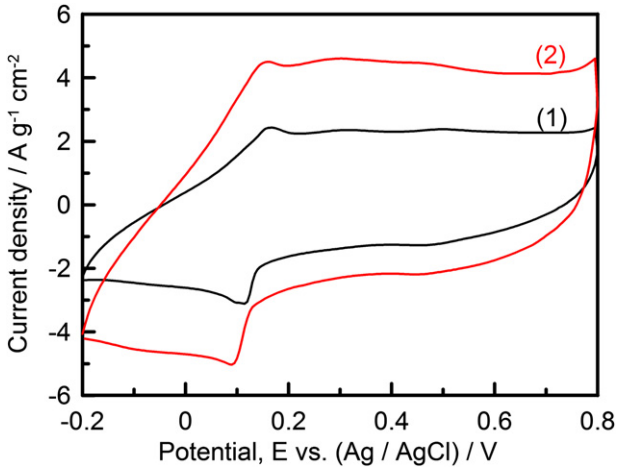

Fig. 4. Cyclic voltammograms (the 2nd cycle) of $VO_x \cdot nH_2O$ synthesized by means of the MAHS method at 140 °C (1) without and (2) with Li-ion doping.

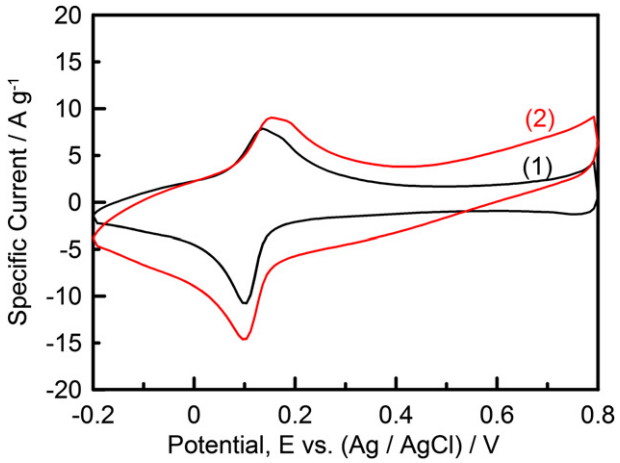

Fig. 5. Cyclic voltammograms (the 500th cycle) of activated $VO_x \cdot nH_2O$ synthesized by means of the MAHS method at 140 °C (1) without and (2) with Li-ion doping.

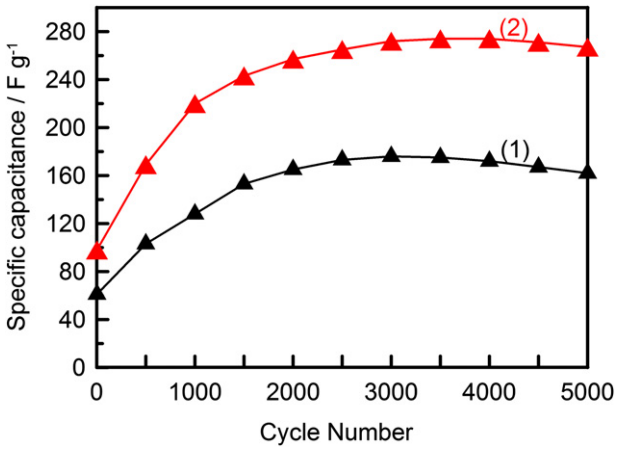

Fig. 6. Dependence of the specific capacitance on the cycle number for $VO_x \cdot nH_2O$ synthesized by means of the MAHS method at 140 °C (1) without and (2) with Li-ion doping.

that the capability of Li-ion intercalation/de-intercalation is significantly enhanced by the Li-ion doping. This enhancement, never reported before, is attributable to a larger spacing between adjacent layers of $VO_x \cdot nH_2O$ (see below), which is favorable for the Li-ion intercalation/de-intercalation in $VO_x \cdot nH_2O$ crystals. Note that the theoretical capacity of a host material for Li-ion intercalation in rechargeable LIBs is fixed [14] and the pre-intercalation of Li ions should reduce the charge storage capacity of the host material. In addition, the intercalation of Li ions into such a host material normally occurs in a relatively narrow potential region [49]. However, due to the fact that the enhancement occurs in the whole potential region of investigation, Li ions should be able to intercalate/de-intercalate in the whole potential region of investigation for both $VO_x \cdot nH_2O$ without and with Li-ion doping. Thus, the Li-ion intercalation mechanism within $VO_x \cdot nH_2O$ may be different from that for rechargeable LIBs although the exact mechanism is unclear.

After the 500-cycle electrochemical activation, a comparison of curves 1 and 2 in Fig. 5 shows three interesting findings. First, the symmetric redox peaks around 0.12 V are obviously found on both curves, revealing the excellent ability of Li-ion intercalation/de-intercalation in both oxides. Second, the CV curves are generally similar in shape while $VO_x \cdot nH_2O$ with doping Li ions possesses much larger current densities. This difference, again, indicates that Li-ion doping in the oxide preparation step significantly enhances the capacity of $VO_x \cdot nH_2O$ for Li-ion intercalation/de-intercalation. Third, both $VO_x \cdot nH_2O$ without and with Li-ion doping show improved electrochemical reversibility for the Li-ion intercalation/de-intercalation after the 500-cycle CV activation process in comparison with the two CV curves in Fig. 4. On the other hand, an oxidation is clearly found on curve 2 at potentials positive than ca. 0.45 V. The exact reason responsible for this phenomenon is unclear, probably due to certain (relatively irreversible) oxidation of V^{4+} into V^{5+} species which seem to be reduced in the negative sweep at potentials negative than the cathodic peak potential. On the other hand, Li-ion doping into $VO_x \cdot nH_2O$ through the MAHS method by adding LiCl in the $VOSO_4 \cdot nH_2O$ precursor solution is effective to promote the electrochemical energy storage ability of $VO_x \cdot nH_2O$.

Curves 1 and 2 in Fig. 6 respectively show the dependence of $C_{S,T}$ on the cycle number of CV for $VO_x \cdot nH_2O$ prepared at 140 °C without and with Li-ion doping. On curve 1, $C_{S,T}$ reaches 73% of its highest value when CV activation reaches 1000 cycles. On curve 2, $C_{S,T}$ even reaches 80% of its highest value under the same cycles of activation. The $C_{S,T}$ further increases to 94% of its highest value for next 1000 cycles. The highest $C_{S,T}$ value of this oxide is 274 F g^{-1} which is much higher than that of $VO_x \cdot nH_2O$ without Li-ion doping (176 F g^{-1}). After the 5000-cycle stability test, the retention remains more than 97% of its highest $C_{S,T}$ value, which is never found before. In 2010, there is an article represents the performance of V_2O_5 in $LiClO_4$ [50] and the cycle life of only 40 cycles. This year, an article about LiV_3O_8 also mentions its cycle life in $LiNO_3$ aqueous solution, but only shows 30 cycles results [51]. 5000 cycles results are really pioneering consequence of vanadium oxide in supercapacitor application in Li-ion based aqueous electrolyte. From the above results and discussion, the rate of electrochemical activation for $VO_x \cdot nH_2O$ with Li-ion doping is obviously faster than that for the sample without doping. In addition, doping Li ions into $VO_x \cdot nH_2O$ through the MAHS method significantly enhances its capacity of Li-ion intercalation/de-intercalation and the charge/discharge cycle-life in the Li-ion supercapacitor application, further demonstrating the unique merits of the MAHS route.

Fig. 7 compares the capacitance retention and the maximal $C_{S,T}$ of $VO_x \cdot nH_2O$ fabricated by the MAHS method at 140 °C with Li-ion doping and by anodic deposition in our previous work [5]. Note that $C_{S,T}$ reaches the highest value (274 F g^{-1}) at ca. the 3000th cycle for $VO_x \cdot nH_2O$ fabricated by the MAHS method while it reaches the

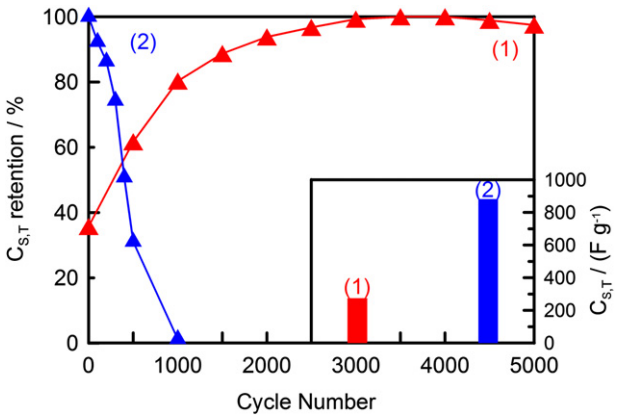

Fig. 7. $C_{S,T}$ retention for $VO_x \cdot nH_2O$ synthesized by (1) the MAHS method at 140 °C with Li-ion doping and (2) the anodic deposition process at 0.4 V; inset shows the corresponding maximal $C_{S,T}$ obtained at about the 3000th and 2nd cycles, respectively.

maximum, 882 F g^{-1}, at the second cycle for that prepared by anodic deposition. The big difference in the maximal $C_{S,T}$ between the above two $VO_x \cdot nH_2O$ should mainly come from the significant differences in morphologies, crystalline quality (discussed before), and contact of $VO_x \cdot nH_2O$ to the current collector. The morphology of $VO_x \cdot nH_2O$ made via the MAHS method is relatively compact, leading to a lower electrolyte-accessible surface area and worse utilization in comparison with that prepared by anodic deposition. Since $VO_x \cdot nH_2O$ powders are synthesized by means of the MAHS method, the contact resistance of drop-coated $VO_x \cdot nH_2O$ powders onto the current collector with 5% binder also decreases the conductivity of whole electrode. On the other hand, $VO_x \cdot nH_2O$ deposits exhibit a good adhesion and contact to the substrate, resulting in good electrode conductivity and an urchin-like morphology which facilitates the penetration of electrolyte. On the other hand, the cycle-life performance of $VO_x \cdot nH_2O$ prepared via MAHS is much better than that produced by means of electrodeposition although $C_{S,T}$ for the former oxide is much lower than that for the latter sample (see inset in Fig. 7), ascribing to the better crystallinity of $VO_x \cdot nH_2O$ prepared via MAHS in comparison with that prepared by anodic deposition.

3.3. Textural characterization of $VO_x \cdot nH_2O$

The above differences in electrochemical properties caused by varying the MAHS temperature and doping Li ions should be linked to the microstructure variation of $VO_x \cdot nH_2O$, which can be identified through materials characterization. Here, all XRD patterns in Fig. 8 reveal that neither the MAHS temperature nor the Li-ion doping can change the crystalline phase of $VO_x \cdot nH_2O$ because they are very similar. These results are consistent with the electrochemical behavior of $VO_x \cdot nH_2O$. Through the Scherrer's equation from the full width at half maximum (FWHM) of the peak centered at 6.1° (2θ), the mean crystal sizes of $VO_x \cdot nH_2O$ synthesized at 140, 180, and 200 °C are equal to 4.2, 4.7, and 6.2 nm, respectively. Moreover, the position of this diffraction peak is slightly shifted from 6.1 to 6.2° with decreasing the MAHS temperature from 200 to 140 °C. Since this peak represents the distance between two adjacent layers of vanadium oxide [1], the worse crystallinity and smaller crystal size probably promote the capacity and rate of the Li-ion intercalation/de-intercalation within $VO_x \cdot nH_2O$ nanocrystals. This finding is consistent with the much higher $C_{S,T}$ of $VO_x \cdot nH_2O$ with worse crystallinity prepared by anodic deposition [5].

Similarly, from a comparison of curves 1 and 4, the distance between two adjacent layers of $VO_x \cdot nH_2O$ is effectively enlarged by this Li-ion doping (with a negative shift in 2θ from 6.2 to 5.9°), resulting in a higher capacity of Li-ion intercalation/de-intercalation within the Li-ion-doped $VO_x \cdot nH_2O$ crystals. A similar result that a strong diffraction line was shifted to a lower 2θ value when Li ions were inserted into vanadium oxide crystals during a discharge process has been reported previously [52]. This report supports the above viewpoint although the doping species in $VO_x \cdot nH_2O$ in this work are hydrated Li ions. Note that Li-ion doping significantly increases the crystal size of $VO_x \cdot nH_2O$ from 4.2 to 9.3 nm. This effect should reduce the capacity and rate of the Li-ion intercalation/de-intercalation while opposite results were found, indicating that effectively enlarging the distance between two adjacent layers of $VO_x \cdot nH_2O$ dominates their Li-ion intercalation/de-intercalation capacity. The successful doping of Li ions has been confirmed through the ICP analysis where the Li/V molar ratio in Li-ion-doped $VO_x \cdot nH_2O$ synthesized at 140 °C is 1/1000. This extremely low Li/V molar ratio has been confirmed by the AES and SIMS analyses (see the supplementary materials). Accordingly, this extremely low content of Li ions in $VO_x \cdot nH_2O$ is proposed to be a doping process. Also note the report [41] that during the discharge process, Li ions will insert into layers of V_2O_5 to form $Li_xV_2O_5$. When x is between 0 and 0.04, the microstructure of $Li_xV_2O_5$ is similar to that of V_2O_5, which can be considered as a layer structure consisting of VO_5 pyramids to form V_2O_5 layers. Hence, the doping of hydrated Li ions in $VO_x \cdot nH_2O$ may be considered as Li-ion insertion on certain sites between oxide layers. Based on this viewpoint and the ICP result, the amount of Li ions doped in $VO_x \cdot nH_2O$ is just between 0 and 0.04, consistent with the layer structure proposal. Therefore, Li ions are considered as a modifier to enlarge the distance between two adjacent oxide layers and to enhance the crystal growth of $VO_x \cdot nH_2O$.

Raman spectrum is used to further investigate the microstructure of $VO_x \cdot nH_2O$ and shows consistent results with those obtained from the XRD patterns. From curves 1 to 3 in Fig. 9, Raman spectra exhibit the same peaks, revealing that the MAHS temperature varying from 140 to 200 °C does not change the crystalline phase of $VO_x \cdot nH_2O$. Based on the FWHM data, a higher MAHS temperature enlarges the crystal size of $VO_x \cdot nH_2O$. In comparison with curve 1, $VO_x \cdot nH_2O$ with Li-ion doping (curve 4) shows a stronger symmetric vibration spectrum, revealing an enhancement in the crystallinity by doping Li ions into the layered structure of $VO_x \cdot nH_2O$. Moreover, the distance between two adjacent layers of $VO_x \cdot nH_2O$ is effectively

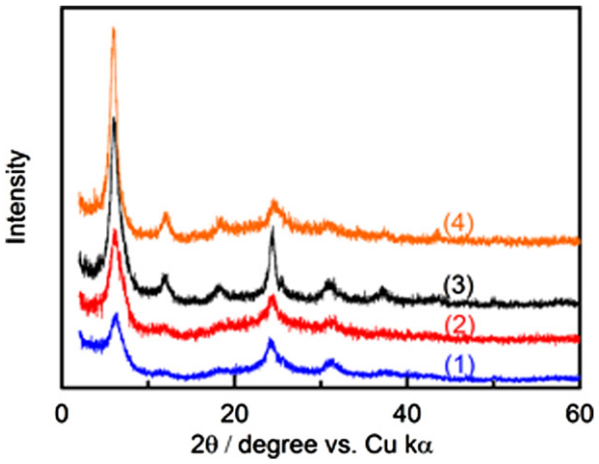

Fig. 8. XRD patterns of $VO_x \cdot nH_2O$ synthesized by means of the MAHS method at (1,4) 140, (2) 180, and (3) 200 °C (1–3) without and (4) with Li-ion doping.

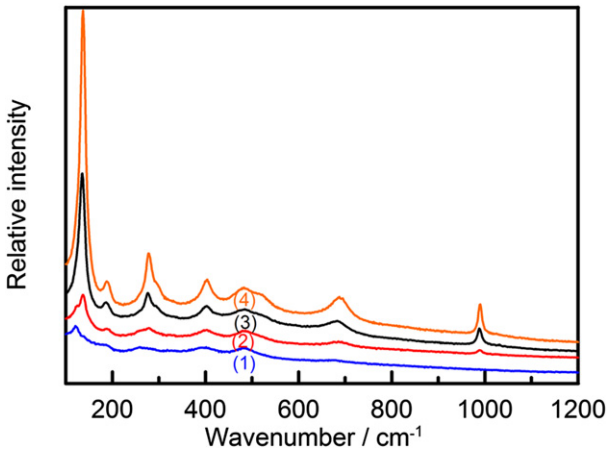

Fig. 9. Raman spectra of $VO_x \cdot nH_2O$ synthesized by means of the MAHS method at (1,4) 140, (2) 180, and (3) 200 °C (1–3) without and (4) with Li-ion doping.

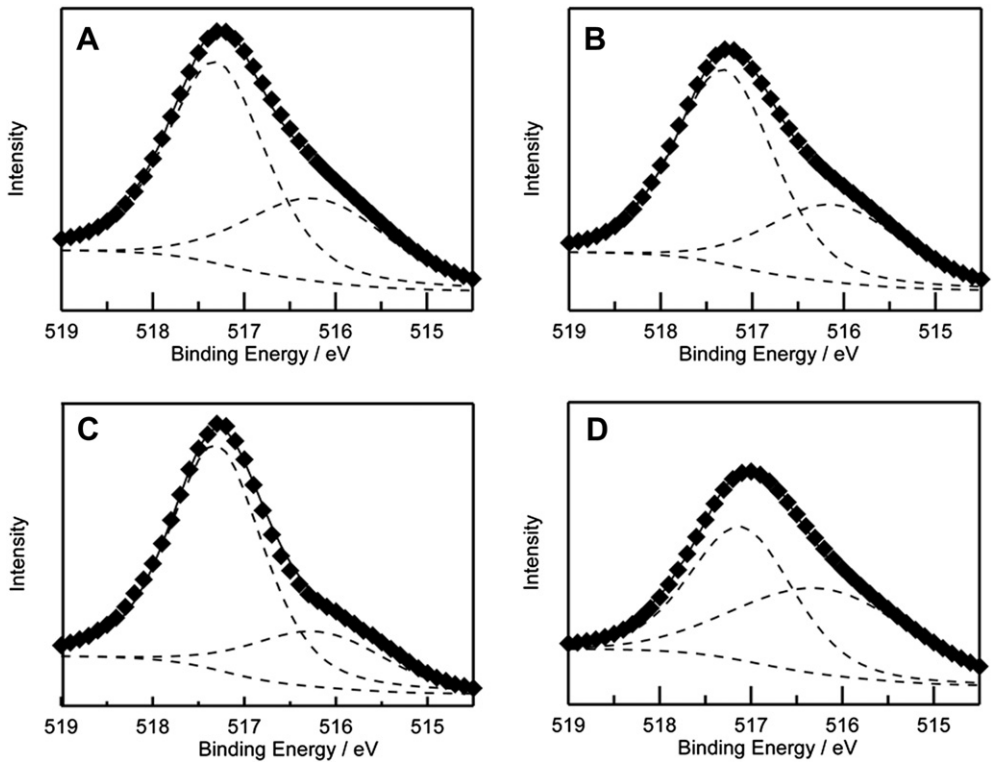

Fig. 10. XPS spectra of $VO_x \cdot nH_2O$ synthesized by means of the MAHS method at (A,D) 140, (B) 180, and (C) 200 °C (A–C) without and (D) with Li-ion doping.

enlarged by the Li-ion doping (see XRD results), reasonably leading to stronger lattice vibration of 136.9 cm^{-1} and 188.2 cm^{-1} which are strongly associated with the layered structure [53]. In fact, a similar phenomenon that the oxide microstructure becomes more ordering with cation intercalation during the discharge process has been reported [2], supporting the above viewpoint.

X-ray photoelectron spectroscopy (XPS) is used to determine the ratio of V^{4+} and V^{5+} in $VO_x \cdot nH_2O$ synthesized at different conditions and typical results are shown in Fig. 10. All V $2p_{3/2}$ spectra in Fig. 10 can be decomposed into two peaks centered at 517.3 and 516.2 eV, corresponding to V^{5+} and V^{4+}, respectively [22,30,54]. Thus, all oxides prepared in this work consist of tetra- and penta-valence vanadium ions. However, the MAHS temperature significantly influences the V^{4+} and V^{5+} ratio of the resultant oxides although the original ratio of V^{4+} and V^{5+} in all precursor solutions is equal to one. Based on the spectra fitting, the quantitative contents of V^{5+} and V^{4+} in all oxides are shown in Table 1. From this table, the content of V^{5+} within $VO_x \cdot nH_2O$ gradually decreases with reducing the MAHS temperature although the difference between $VO_x \cdot nH_2O$ synthesized at 180 and 140 °C may be considered as an error. More importantly, the amount of V^{5+} is approximately equal to that of V^{4+} when $VO_x \cdot nH_2O$ was synthesized at 140 °C with doping Li ions. The exact reasons why $VO_x \cdot nH_2O$ synthesized at a higher MAHS temperature contains a higher content of V^{5+} are not clear, while dissolved oxygen molecules in the precursor solution may further oxidize the tetra-valence vanadium ions into penta-valence ions during the MAHS process. Since inserting Li ions into $VO_x \cdot nH_2O$ should reduce the mean oxidation state of V species in the oxide [55], doping Li ions into the nanocrystals of $VO_x \cdot nH_2O$ reasonably inhibits the oxidation of vanadium species during the MAHS process. Also note that the V^{5+}/V^{4+} ratio of $VO_x \cdot nH_2O$ with Li-ion doping, synthesized at 140 °C, is very close to that of $VO_x \cdot nH_2O$ fabricated by anodic deposition at 0.4 V versus an Ag/AgCl electrode [5,33]. Furthermore, $VO_x \cdot nH_2O$ was found to exhibit a higher capacity and a better electrochemical reversibility for Li-ion intercalation/de-intercalation when this oxide contained more V^{4+} [5,33]. The above interesting consistency is believed to be one of the reasons why this $VO_x \cdot nH_2O$ with Li-ion doping shows much better capacitive performances than all oxides without doping.

Table 1
The molar ratio of penta- and tetra-valence vanadium ions within $VO_x \cdot nH_2O$ synthesized by means of the MAHS method under different conditions.

Specimen (V:Li)	V^{5+}/V^{4+}
200 °C (1:0)	74.1:25.9
180 °C (1:0)	68.4:31.6
140 °C (1:0)	67.2:32.8
140 °C (1:1)	51.6:48.4

4. Conclusions

Vanadium oxides ($VO_x \cdot nH_2O$) with excellent capacitive performances can be synthesized easily and rapidly by means of the microwave-assisted hydrothermal synthesis method. The crystalline structure of $VO_x \cdot nH_2O$ is not changed by varying the MAHS temperature and adding LiCl in the precursor solution. However, the crystal size and the spacing distance between two adjacent oxide layers are significantly affected by the above two variables, resulting in the great influences on the Li-ion intercalation/de-intercalation capacity and rate within $VO_x \cdot nH_2O$ nano-crystals. The lower MAHS temperature is applied, the lower V^{5+}/V^{4+} ratio in $VO_x \cdot nH_2O$ is obtained. The V^{5+}/V^{4+} ratio also decreases with the doping of Li ions in $VO_x \cdot nH_2O$. Doping Li ions into $VO_x \cdot nH_2O$ not only enlarges the spacing distance between adjacent oxide layers and the crystal size of $VO_x \cdot nH_2O$ but also enhances its specific

capacitance and prolongs its cycle life in the Li-ion supercapacitor application.

Acknowledgment

The financial support of this work, by the National Science Council of the ROC Taiwan under contract nos. NSC 98-2221-E-007-078-MY3, 101-3113-E-006-010, and the boost program from the Low Carbon Energy Research Center in National Tsing Hua University, is gratefully acknowledged.

References

[1] S. Nordlinder, L. Nyholm, T. Gustafsson, K. Edstrom, Chem. Mater. 18 (2006) 495.
[2] S. Tepavcevic, H. Xiong, V.R. Stamenkovic, X. Zuo, M. Balasubramanian, V.B. Prakapenka, C.S. Johnson, T. Rajh, ACA Nano 6 (2012) 530.
[3] Q.-T. Qu, Y. Shi, L.-L. Li, W.-L. Guo, Y.-P. Wu, H.-P. Zhang, S.-Y. Guan, R. Holze, Electrochem. Commun. 11 (2009) 1325.
[4] O.Y. Posudievsky, O.A. Kozarenko, V.S. Dyadyun, S.W. Jorgensen, J.A. Spearot, V.G. Koshechko, V.D. Pokhodenko, J. Power Sources 196 (2011) 3331.
[5] J.-M. Li, K.-H. Chang, C.-C. Hu, Electrochem. Commun. 12 (2010) 1800.
[6] C.-C. Hu, C.-M. Huang, K.-H. Chang, J. Power Sources 185 (2008) 1594.
[7] R. Kotz, M. Carlen, Electrochim. Acta 45 (2000) 2483.
[8] B.E. Conway, J. Electrochem. Soc. 138 (1991) 1539.
[9] B.E. Conway, V. Birss, J. Wojtowicz, J. Power Sources 66 (1997) 1.
[10] B.E. Conway, Electrochemical Supercapacitors, Kluwer-Plenum Pub. Co., New York, 1999.
[11] B. Andrew, J. Power Sources 91 (2000) 37.
[12] Y.-S. Hu, X. Liu, J.-O. Müller, R. Schlögl, J. Maier, D.S. Su, Angew. Chem. Int. Ed. 48 (2009) 210.
[13] T. Watanabe, Y. Ikeda, T. Ono, M. Hibino, M. Hosoda, K. Sakai, T. Kudo, Solid State Ionics 151 (2002) 313.
[14] Y. Wang, K. Takahashi, K.H. Lee, G.Z. Cao, Adv. Funct. Mater. 16 (2006) 1133.
[15] A. Pan, D. Liu, X. Zhou, B.B. Garcia, S. Liang, J. Liu, G. Cao, J. Power Sources 195 (2010) 3893.
[16] K. Takahashi, S.J. Limmer, Y. Wang, G.Z. Cao, J. Phys. Chem. B 108 (2004) 9795.
[17] Z. Wang, J. Chen, X. Hu, Thin Solid Films 375 (2000) 238.
[18] P. Liu, S.-H. Lee, C.E. Tracy, J.A. Turner, J.R. Pitts, S.K. Deb, Solid State Ionics 165 (2003) 223.
[19] A. Jin, W. Chen, Q. Zhu, Y. Yang, V.L. Volkov, G.S. Zakharova, Thin Solid Films 517 (2009) 2023.
[20] J.-F. Liu, X. Wang, Q. Peng, Y.-D. Li, Adv. Mater. 17 (2005) 764.
[21] K. Honma, M. Yoshinaka, K. Hirota, O. Yamaguchi, J. Asai, Y. Makiyama, Mater. Res. Bull. 31 (1996) 531.
[22] K.-H. Chang, C.-C. Hu, Acta Mater. 55 (2007) 6192.
[23] Z. Chen, Y. Qin, D. Weng, Q. Xiao, Y. Peng, X. Wang, H. Li, F. Wei, Y. Lu, Adv. Funct. Mater. 19 (2009) 3420.
[24] Y. Yang, Q. Zhu, A. Jin, W. Chen, Solid State Ionics 179 (2008) 1250.
[25] C. Chang, J. Xiang, X. Shi, X. Han, L. Yuan, J. Sun, Electrochim. Acta 54 (2008) 623.
[26] C.V.S. Reddy, S.-I. Mho, R.R. Kalluru, Q.L. Williams, J. Power Sources 179 (2008) 854.
[27] C.-C. Hu, K.-H. Chang, Electrochem. Solid-State Lett. 7 (2004) A400.
[28] F. Sediri, F. Touati, N. Gharbi, Mater. Lett. 61 (2007) 1946.
[29] L. Yu, X. Zhang, Mater. Chem. Phys. 87 (2004) 168.
[30] C. Ban, M.S. Whittingham, Solid State Ionics 179 (2008) 1721.
[31] N. Pinna, U. Wild, J. Urban, R. Schlögl, Adv. Mater. 15 (2003) 329.
[32] N. Pinna, M. Willinger, K. Weiss, J. Urban, R. Schlogl, Nano Lett. 3 (2003) 1131.
[33] J.-M. Li, K.-H. Chang, C.-C. Hu, Electrochim. Acta 55 (2010) 8600.
[34] C.-M. Huang, C.-C. Hu, K.-H. Chang, J.-M. Li, Y.-F. Li, J. Electrochem. Soc. 156 (2009) A667.
[35] M. Jayalakshmi, M.M. Rao, N. Venugopal, K.-B. Kim, J. Power Sources 166 (2007) 578.
[36] K. West, B. Zachau-Christiansen, T. Jacobsen, S. Skaarup, Solid State Ionics 76 (1995) 15.
[37] K. West, B. Zachau-Christiansen, S.V. Skaarup, F.W. Poulsen, Solid State Ionics 57 (1992) 41.
[38] Y. Sato, T. Nomura, H. Tanaka, K. Kobayakawa, J. Electrochem. Soc. 138 (1991) L37.
[39] E. Potiron, A.L. La Salle, A. Verbaere, Y. Piffard, D. Guyomard, Electrochim. Acta 45 (1999) 197.
[40] E. Shembel, R. Apostolova, V. Nagirny, D. Aurbach, B. Markovsky, J. Power Sources 81–82 (1999) 480.
[41] W.-C. Fang, W.-L. Fang, Chem. Commun. 44 (2008) 5236.
[42] Z.-J. Lao, K. Konstantinov, Y. Tournaire, S.H. Ng, G.X. Wang, H.K. Liu, J. Power Sources 162 (2006) 1451.
[43] S. Komarneni, R. Roy, Q.H. Li, Mater. Res. Bull. 27 (1992) 1393.
[44] S. Komarneni, Q. Li, K.M. Stefansson, R. Roy, J. Mater. Res. 8 (1993) 3176.
[45] K.-H. Chang, C.-C. Hu, C.-M. Huang, Y.-L. Liu, C.-I. Chang, J. Power Sources 196 (2011) 2387.
[46] Y.-L. Yang, C.-C. Hu, C.-C. Hua, CrystEngComm 13 (2011) 5638.
[47] C.-C. Hu, Y.-L. Yang, T.-C. Lee, Electrochem. Solid-State Lett. 13 (2010) A173.
[48] K. Lee, G. Cao, J. Phys. Chem. B 109 (2005) 11880.
[49] M.D. Levi, Z. Lu, D. Aurbach, J. Power Sources 97–98 (2001) 482.
[50] D. Yu, C. Chen, S. Xie, Y. Liu, K. Park, X. Zhou, Q. Zhang, J. Li, G. Cao, Energy Environ. Sci. 4 (2011) 858.
[51] H. Yadegari, A. Jabbari, H. Heli, J. Solid State Electrochem. 16 (2012) 227.
[52] R. Baddour-Hadjean, V. Golabkan, J.P. Pereira-Ramos, A. Mantoux, D. Lincot, J. Raman Spectrosc. 33 (2002) 631.
[53] S.-H. Lee, H.-M. Cheong, M. Je Seong, P. Liu, C.E. Tracy, A. Mascarenhas, J.R. Pitts, S.K. Deb, J. Appl. Phys. 92 (2002) 1893.
[54] C. Ban, N.A. Chernova, M.S. Whittingham, Electrochem. Commun. 11 (2009) 522.
[55] J.S. Braithwaite, C.R.A. Catlow, J.D. Gale, J.H. Harding, Chem. Mater. 11 (1999) 1990.